Chem. Mater. **2008,** *20,* 5610–5621

B3LYP Simulation of the Full Vibrational Spectrum of 45S5 Bioactive Silicate Glass Compared to *v*-Silica

Marta Corno,[†] Alfonso Pedone,[‡] Roberto Dovesi,[†] and Piero Ugliengo*,[†]

Department of IFM Chemistry, NIS Centre of Excellence and INSTM (Materials Science and Technology) National Consortium, University of Torino, Via P. Giuria 7, Torino, Italy, Department of Chemistry, University of Modena and Reggio Emilia, Via G. Campi 183, 41100 Modena, Italy

Received April 29, 2008. Revised Manuscript Received July 1, 2008

The IR spectrum of the Bioglass 45S5 (of composition 46.1 SiO_2, 24.4 Na_2O, 26.9 CaO, and 2.6 P_2O_5 mol %) has been simulated by means of periodic ab initio B3LYP calculations. The initial glass structure unit cell envisaging 78 atoms was generated through a melt quench process by means of classical molecular dynamics simulations. The molecular mechanics optimized unit cell has then been fully reoptimized (both unit-cell parameters and internal coordinates) at B3LYP level in a periodic approach using Gaussian basis sets of double-ζ quality by means of the CRYSTAL06 code. Although long-range structural properties cannot be modeled by using this ab initio approach because of the intrinsic amorphous nature of the glass, the quantum mechanical simulation proved to be extremely effective in predicting and analyzing the vibrational features of this biomaterial. The effect of modifiers Na and Ca cations on the network dynamics has been assessed by comparing the 45S5 vibrational spectrum with that of amorphous v-SiO_2, both simulated at the B3LYP level. A detailed assignment of each spectral peak to the corresponding vibrational mode of the two glasses has been addressed and the role of cation modifiers on the vibrational features has been analyzed in greater details. This may be useful to support further IR and Raman investigations of the bulk structure of these materials.

Introduction

Surface-active silicate glasses with the addition of calcium and phosphorus have been widely used in restorative and regenerative medical applications since their discovery in the early 1970s by Hench and co-workers.[1−5] In a pioneering work, Hench showed the formation of strong bonds between the famous 45S5 Bioglass (of composition 46.1 SiO_2, 24.4 Na_2O, 26.9 CaO, and 2.6 P_2O_5 mol %) and rats' femurs. Bioactive glasses show a strong active response after they are implanted in the human body or put in contact with acellular simulated body fluid (SBF).[6] A series of chemical transformations occurs after implantation, which leads to the growth of a layer of crystalline hydroxyl-carbonate apatite (HCA) on their surface. This layer then interacts with and incorporates biomolecules such as collagen, whereas further cellular steps lead to a strong and stable chemical bond between the glass and human hard (bone) and, in some cases, soft (muscles) tissues.

Because the rate at which the HCA crystallization occurs is crucial for the success of biomedical applications, the bioactivity of these glasses is often measured in terms of the rate of HCA formation. The mechanism of HCA formation has been roughly explained in the following steps: (a) initial leaching of Na^+ ions, which are replaced by H^+ from solution; (b) breaking of Si−O−Si bonds and release of soluble silica $Si(OH)_4$ to the solution; (c) the surface silanol groups formed in both the previous steps condense to form a silica-rich layer depleted of Na^+ and Ca^{2+} ions on the surface; (d) calcium and phosphate ions are released through this surface layer and incorporate other Ca^{2+} and PO_4^{3-} from solution and crystallize to HCA.[3]

By altering the glass composition, one can in principle tune the rate of HCA formation and the glass physical properties for a specific application; however, a more rational control of the bioactivity could be achieved by establishing the microscopic, structural basis for the bioactive behavior and its relation with the composition.

Compared to a fully interconnected silicate network, such as vitreous silica, the inclusion of modifier oxides such as Na_2O and CaO leads to the breaking of Si−BO−Si bonds (where BO is a bridging oxygen) and their replacement by Si−NBO···M bonds (where NBO is a nonbridging oxygen, and M is a Na or Ca cation). At high concentrations, the modifiers percolate through the bulk of the glass and form a network of pathways, or channels, that play the key role in the structural, elastic, and transport properties of glasses.

An important issue in bioglass science involves the partial incorporation of phosphate units into the silicate network,[7−9] which may affect the phosphate release rate.

Among the standard solid-state experimental techniques, nuclear magnetic resonance (NMR),[7,10−12] Raman[9,13] and

---

* Corresponding author. E-mail: piero.ugliengo@unito.it.
[†] University of Torino.
[‡] University of Modena and Reggio Emilia.

(1) Hench, L. L. *Science* **1980**, *208*, 826.
(2) Hench, L. L. *Biomaterials* **1998**, *19*, 1419.
(3) Hench, L. L.; Splinter, R. J.; Allen, W. C.; Greenlee, T. K. *J. Biomed. Mater. Res. Symp.* **1971**, *2*, 117.
(4) Hench, L. L.; Wilson, J. *Science* **1984**, *226*, 630.
(5) Hench, L. L.; Wilson, J. *An Introduction to Bioceramics*; World Scientific: Singapore, 1993.
(6) Kokubo, T.; Kushitani, H.; Sakka, S. *J. Biomed. Mater. Res. Symp.* **1990**, *24*, 721.

10.1021/cm801164u CCC: $40.75

infrared spectroscopy[14] are frequently employed to probe the structural features of different bioglasses compositions and to highlight the structural changes that characterize bioactivity.

These techniques have revealed that the medium range order of the 45S5 Bioglass is characterized by a very open silicate network dominated by Q^2 and Q^3 species (a Q^n species is a network-forming ion bonded to n bridging oxygens).

The existence of more than two different Q^n species of silicon for glasses with compositions similar to that of 45S5 glass is the subject of active debate; a source of uncertainty is the intrinsic difficulty in detecting species such as Q^1 and Q^4 present at low concentration, whose signal partially overlaps with the signal of the predominating Q^n sites. Although a binary model (with only Q^2 and Q^3 species) is sometimes assumed,[10,12] other experimental data have been interpreted with up to four Q^n (from Q^1 to Q^4) species simultaneously present.[7,9,11]

It is normally assumed that phosphate groups are predominantly isolated orthophosphates associated with modifier M ions. Indeed, only Q^0(P) are reported in some NMR studies;[10,12] on the other hand, cross-linking between silicate and phosphate groups has sometimes been proposed to interpret IR, Raman, and other NMR data,[7−9,11,15] although the occurrence of Si−O−P links at very low phosphate levels is not clear-cut.

The microscopic structure of this material has been explored in higher detail by several classical molecular dynamics simulations by using both the rigid ionic model[11,16,17] and the shell-model[18−20]and with quantum-mechanical simulations by Carr−Parrinello molecular dynamics simulations[21,22] and the energy minimization method included in CRYSTAL06 code.[16,23] The coordination environment of network formers and modifiers,[16,24] the tendency to form clusters and inhomogeneities,[20,25] the occurrence of chain and ring nanostructures,[19] and the effect of phosphorus inclusion were discussed in relation to bioactivity[18] and medium-range order.[11] All these methods showed to be in perfect agreement in reproducing short-range geometrical features such as the coordination and bond distances of network formers and modifiers.[16,26] Little differences were obtained in the structural parameters commonly used to describe the medium range order in amorphous glasses such as Si−O−Si and Si−O−P angles and Q^n distributions. In fact, molecular dynamics simulations using the rigid ionic model overestimate the Si−O−Si and Si−O−P intertetrahedral angles with respect to molecular dynamics simulations performed with the shell-model, static QM methods, and Carr−Parrinello molecular dynamics. This leads to worse Q^n distributions compared to experimental data. However, the rigid ionic model does show that the silicon is dominated by Q^2 and Q^3 species.

In almost all the works mentioned above, in which the models of the 45S5 glass were obtained by classical MD quench from the melt, a common finding is the presence of a relevant fraction of Q^1 phosphate groups forming one P−O−Si link with an adjacent silicate. In a recent work[22] Tilocca generated a glass structure using a full-CPMD quench that also incorporated P−O−Si links; despite the limited statistics due to small system size, this does seem to confirm that these links are an important structural feature of bioactive silicate glasses, as their presence in the full ab initio structure rules out a possible bias on their occurrence due to the use of empirical potentials to generate the glass.

The majority of the previous works was devoted to the analysis of structural properties, whereas a detailed study of dynamical properties has not been addressed except for the calculation of the vibrational density of states by Fourier transforming of the velocity autocorrelation function calculated from CPMD trajectories.[22,24] However, vibrational properties and the IR spectrum of a complex material such as 45S5 glass can be simulated nowadays fully ab initio by means of modern quantum-mechanical codes like CRYSTAL06.[23] This is a periodic ab initio program based on an atom centered (Gaussian) basis set and has been successfully applied to calculate the electronic properties of various crystalline materials.[27,28] The recent implementation of analytical energy gradients[29,30] has provided an important

---

(7) Clayden, N. J.; Pernice, P.; Aronne, A. *J. Non-Cryst. Solids* **2005**, *351*, 195.
(8) Li, D.; Fleet, M. E.; Bancroft, G. M.; Kasrai, M.; Pan, Y. *J. Non-Cryst. Solids* **1995**, *188*, 181.
(9) Lin, C. C.; Huang, L. C.; Shen, P. *J. Non-Cryst. Solids* **2005**, *351*, 3195.
(10) Elgayar, I.; Aliev, A. E.; Bocaccini, A. R.; Hill, R. G. *J. Non-Cryst. Solids* **2005**, *351*, 173.
(11) Linati, L.; Lusvardi, G.; Malavasi, G.; Menabue, L.; Menziani, M. C.; Mustarelli, P.; Pedone, A.; Segre, U. *J. Non-Cryst. Solids* **2008**, *354*, 84.
(12) Lockyer, M. W. G.; Holland, D.; Dupree, R. *J. Non-Cryst. Solids* **1995**, *188*, 207.
(13) Oliveira, J. M.; Correia, R. N.; Fernandes, M. H. *Biomaterials* **2002**, *23*, 371.
(14) ElBatal, H. A.; Azooz, M. A.; Khalil, E. M. A.; Soltan Monem, A.; Hamdy, Y. M. *Mater. Chem. Phys.* **2003**, *80*, 599.
(15) Linati, L.; Lusvardi, G.; Malavasi, G.; Menabue, L.; Menziani, M. C.; Mustarelli, L. P.; Segre, U. *J. Phys. Chem. B* **2005**, *109*, 4989.
(16) Malavasi, G.; Menziani, M. C.; Pedone, A.; Civalleri, B.; Corno, M.; Ugliengo, P. *Theor. Chem. Acc.* **2007**, *117*, 933.
(17) Pedone, A.; Malavasi, G.; Menziani, M. C.; Cormack, A. N.; Segre, U. *J. Phys. Chem. B* **2006**, *110*, 11780.
(18) Tilocca, A.; Cormack, A. N. *J. Phys. Chem. B* **2007**, *111*, 14256.
(19) Tilocca, A.; Cormack, A. N.; de Leeuw, N. H. *Faraday Discuss.* **2007**, *136*, 45.
(20) Tilocca, A.; Cormack, A. N.; de Leeuw, N. H. *Chem. Mater.* **2007**, *19*, 95.
(21) Tilocca, A.; de Leeuw, N. H. *J. Mater. Chem.* **2006**, *16*, 1950.
(22) Tilocca, A. *Phys. Rev. B* **2007**, *76*, 224202.
(23) Dovesi, R.; Saunders, V. R.; Roetti, C.; Orlando, R.; Zicovich-Wilson, C. M.; Pascale, F.; Civalleri, B.; Doll, K.; Harrison, N. M.; Bush, I. J.; D'Arco, P.; Llunell, M. *CRYSTAL2006 User's Manual*; University of Turin: Torino, Italy, 2006; http://www.crystal.unito.it.
(24) Tilocca, A.; de Leeuw, N. H. *J. Phys. Chem. B* **2006**, *110*, 51.
(25) Lusvardi, G.; Malavasi, G.; Menabue, L.; Menziani, M. C.; Pedone, A.; Segre, U. *J. Phys. Chem. B* **2005**, *109*, 21586.
(26) Pedone, A. *Computer Simulations of Chemical Physical Properties of Amorphous Inorganic Materials.* Ph.D Thesis, University of Modena and Reggio Emilia, Modena, Italy, 2008.
(27) Dovesi, R.; Civalleri, B.; Orlando, R.; Roetti, C.; Saunders, V. R. Ab Initio Quantum Simulation in Solid State Chemistry. In *Review in Computational Chemistry*; Lipkowitz, K. B., Larter, R., Cundari, T. R., Eds.; John Wiley & Sons: New York, 2005; Vol *21*; p 1.
(28) Dovesi, R.; Orlando, R.; Civalleri, B.; Roetti, C.; Saunders, V. R.; Zicovich-Wilson, C. M. *Z. Kristallogr.* **2005**, *220*, 571.
(29) Doll, K. *Comput. Phys. Commun.* **2001**, *137*, 74.
(30) Doll, K.; Saunders, V. R.; Harrison, N. M. *Int. J. Quantum Chem.* **2001**, *82*, 1.

tool to study the structural changes[31] and vibrational properties of crystalline compounds.[32,33]

In particular, the calculation of vibrational modes is a remarkable new feature that allows us to highlight the specific contribution of the structural units within the glass, such as different Q^n distribution sites and for identifying possible markers of P−O−Si linkages.

In this work, the assignment of the computed frequencies for the 45S5 Bioglass structure has been carried out by means of several complementary methodologies: (i) the isotopic substitutions of the atoms in the unit cell to decouple frequencies which allow to distinguish different regions in the simulated IR spectrum; (ii) the potential energy distribution analysis as encoded in the CRYSTAL06 code; and (iii) the graphical visualization of the displacements associated with the eigenvectors of each mode. Finally, the IR spectrum and the vibrational density of states (VDOS) of 45S5 Bioglass have been compared to those calculated for vitreous silica (v-SiO$_2$) at the B3LYP level and experiments when available. This is useful for inferring the effects of the cation modes on the dynamics of the silica network.

Computational Methods

Glass Generation. The glass sample has been generated by means of classical MD simulations by using an empirical partial charge rigid ionic model, which has been shown to well-reproduce the structure, transport, and mechanical properties of oxides, silicates, and silica-based glasses.[34−38] A cubic box containing 78 atoms of $Na_{12}Ca_7P_2Si_{13}O_{44}$ composition and cell size of 10.10 Å per side, calculated accordingly with the experimental density of 2.72 g/cm^3, has been considered.[16] The initial positions of each atom were randomly generated. The leapfrog Verlet integrator and a time step of 2 fs has been used to perform MD simulations with the GULP package.[39] The system was then heated at 6000 K. The melt was then equilibrated for 100 ps and subsequently cooled continuously from 6000 to 300 K in 1140 ps with a nominal cooling rate of 5 K/ps. The temperature was decreased by 0.01 K every time step using Nose-Hoover thermostat[40] with the time constant parameter for the frictional coefficient set to 0.1 ps. Simulations were carried out in the constant volume NVT ensemble. Other 100 ps of equilibration at constant volume and 50 ps of data production were performed at 300 K.

Finally, static energy minimizations at constant P and constant V were carried out on the obtained MD configurations.[16] The one chosen as a starting point for the periodic ab initio full geometry relaxation is considered to be representative of the different structural features observed for the constituting atoms during the glass forming dynamic procedure. This is a common procedure in ab initio calculations of glasses[21,41−43] and enables only short-range relaxations at the ab initio level, whereas the medium-range structure, such as the connectivity of the glass-forming sites, is "frozen" to the initial configuration obtained by classical MD. It has been recently shown that a full ab initio molecular dynamics of the melt-quench process considerably improves the agreement with experiment of the Q^n distribution for lithium silicate glasses[44] and for the 45S5 glass.[22] However, in both these works, it was shown that the vibrational density of states of the glass obtained fully ab initio is very similar to the VDOS calculated using a mixed classical-CPMD approach, showing that the small structural differences of the glass samples obtained do not affect their vibrational features.

As initial starting structure for v-SiO$_2$, we used a 72-atom supercell generated by using the Monte Carlo bond-switching method and relaxed at DFT level by Bakos et al.[45,46]

Quantum-Mechanical Calculations. In the present work, all the quantum mechanical calculations about 45S5 Bioglass and v-SiO$_2$ have been performed with the ab initio CRYSTAL06 code,[23] running on standard Linux PC, which implements the Hartree−Fock and Kohn−Sham self-consistent field method for the study of periodic systems. All graphical inspections have been carried out with the molecular graphics program MOLDRAW.[47]

Hamiltonian and Computational Parameters. The Becke three-parameter (B3) hybrid exchange functional in combination with the gradient-corrected correlation functional (LYP) of Lee, Yan, and Parr[48,49] has been used both for the geometry optimization[16] and for the phonon frequency calculation. The B3LYP functional has recently been proved to be very accurate for the treatment of ionic and covalent crystals[50] and has been used by some of us to study complex silicates,[27] both as far as structures and phonons frequencies are concerned.[32,51,52] Phonon spectrum at Γ point for the hydroxyapatite (HA) crystal has also been recently computed by some of us,[53] with a level of accuracy within 30−80 cm^{-1}. Because of the complexity of HA material, it is expected that a similar accuracy also holds here for the case of Hench's bioglass.

The adopted grid of points, over which the integration of electronic density and its gradient is performed, was a pruned grid of 75 radial points and 434 angular points, divided into 5 subintervals of 50, 146, 194, 434, and 194 points (known as LGRID) resulting in about 900 000 total grid points. With this grid, the integration of the electronic density gives the total number of electron with an error of 1×10^{-3} electrons upon 766 total in the unit cell. For all calculations, default values of Coulomb and

---

(31) Civalleri, B.; D'Arco, P.; Orlando, R.; Saunders, V. R.; Dovesi, R. *Chem. Phys. Lett.* **2001**, *348*, 131.

(32) Pascale, F.; Zicovich-Wilson, C. M.; Lopez Gejo, F.; Civalleri, B.; Orlando, R.; Dovesi, R. *J. Comput. Chem.* **2004**, *25*, 888.

(33) Zicovich-Wilson, C. M.; Pascale, F.; Roetti, C.; Saunders, V. R.; Orlando, R.; Dovesi, R. *J. Comput. Chem.* **2004**, *25*, 1873.

(34) Pedone, A.; Malavasi, G.; Cormack, A. N.; Segre, U.; Menziani, M. C. *Chem. Mater.* **2007**, *19* (13), 3144.

(35) Pedone, A.; Malavasi, G.; Cormack, A. N.; Segre, U.; Menziani, M. C. *Theor. Chem. Acc.* **2008**, DOI:10.1007/s00214−008−0434−7.

(36) Pedone, A.; Malavasi, G.; Menziani, M. C.; Cormack, A. N.; Segre, U. *J. Phys. Chem. B* **2006**, *110*, 11780.

(37) Pedone, A.; Malavasi, G.; Menziani, M. C.; Segre, U.; Cormack, A. N. Submitted to *J. Phys. Chem.*

(38) Pedone, A.; Malavasi, G.; Menziani, M. C.; Segre, U.; Cormack, A. N. Submitted to *Chem. Mater.*

(39) Gale, J. D.; Rohl, A. L. *Mol. Simul.* **2003**, *29*, 291.

(40) Hoover, W. G. *Phys. Rev. A* **1985**, *31*, 1695.

(41) Donadio, D.; Bernasconi, M.; Tassone, F. *Phys. Rev. B* **2004**, *70*, 214205.

(42) Ispas, S.; Benoit, M.; Jund, P.; Jullien, R. *Phys. Rev. B* **2001**, *64*, 214206.

(43) Van Ginhoven, R. M.; Jonsson, H.; Corrales, L. R. *Phys. Rev. B* **2005**, *71*, 024208.

(44) Du, J.; Corrales, L. R. *J. Chem. Phys.* **2006**, *125*, 114702.

(45) Bakos, T.; Rashkeev, S. N.; Pantelides, S. T. *Phys. Rev. Lett.* **2002**, *88*, 055508.

(46) Bakos, T.; Rashkeev, S. N.; T., P. S. *IEEE Trans. Nucl. Sci.* **2002**, *49*, 2713.

(47) Ugliengo, P. MOLDRAW: A molecular graphics program to display and manipulate molecular structures, H1 (32-bit) ed.; University of Turin: Torino, Italy, 2005; http://www.moldraw.unito.it.

(48) Becke, A. D. *J. Chem. Phys.* **1993**, *98*, 5648.

(49) Lee, C.; Yang, W.; Parr, R. G. *Phys. Rev. B* **1988**, *37*, 785.

(50) Corà, F.; Alfredsson, M.; Mallia, G.; Middlemiss, D. S.; Mackrodt, W. C.; Dovesi, R.; Orlando, R. *Struct. Bonding* **2004**, *113*, 171.

(51) Pascale, F.; Ugliengo, P.; Civalleri, B.; Orlando, R.; D'Arco, P.; Dovesi, R. *J. Chem. Phys.* **2002**, *117*, 5337.

(52) Pascale, F.; Zicovich-Wilson, C. M.; Orlando, R.; Dovesi, R. *J. Phys. Chem. B* **2005**, *109*, 6146.

(53) Corno, M.; Busco, C.; Civalleri, B.; Ugliengo, P. *Phys. Chem. Chem. Phys.* **2006**, *8*, 2464.

exchange tolerances series have been used (ITOL1 = ITOL2 = ITOL3 = ITOL4 = 6, ITOL5 = 12); Hamiltonian matrix has been diagonalized on 14 reciprocal lattice points (k-points, shrinking factor IS = 2).[54]

Basis Set. The basis set adopted is an all-electron extended Gaussian-type function (GTF) basis set.[16] For Ca ions, the first 10 electrons (shell 1 and 2) are represented by the effective core pseudopotential of Hay and Wadt,[55,56] while three contracted GTF are used for the remaining 10 electrons (shell orbital 3sp and 4s) and one GTF for the outer sp shell (basis [HAYWSC]-31G).[57] The exponent of the most diffuse shell is $\alpha_{sp} = 0.5$ bohr^{-2}. Na ions are described by a 8−511G basis set (most diffuse shell exponents $\alpha_{sp} = 0.323$ bohr^{-2}).[58−62] Si atoms adopt a 6−21G(d) modified basis set (most diffuse shell exponent $\alpha_{sp} = 0.13$ and $\alpha_d = 0.5$ bohr^{-2} for polarization functions), whereas P atoms are described by a 85−21G(d) basis set with most diffuse shell exponent $\alpha_{sp} = 0.135$ bohr^{-2} and $\alpha_d = 0.74583$ bohr^{-2} for polarization, respectively. Oxygen atoms are described with a 6−31G(d) basis set with the most diffuse shell exponents $\alpha_{sp} = 0.2742$ bohr^{-2} and $\alpha_d = 0.538$ bohr^{-2} for polarization. The total number of atomic orbitals amounts to 1098 functions.

Vibrational Frequencies and IR Spectra. Phonon frequencies of Bioglass 45S5 and v-SiO$_2$ have been calculated as the eigenvalues obtained by diagonalizing the weighted Hessian matrix associated with Γ point (point $k = 0$ in the first Brillouin zone, called central zone, IR and RAMAN spectra refer to this point) in the harmonic approximation.

The mass-weighted Hessian matrix was obtained by numerical differentiation of the analytical first derivative, calculated at geometries obtained by incrementing in turn each of the 3N nuclear coordinates by a small amount u with respect to the equilibrium geometry. The reader can refer to a recent paper for a complete discussion of the computational conditions and other numerical aspects concerning the calculation of the vibrational frequencies at Γ point.[32]

Along with harmonic frequencies and their symmetry character, CRYSTAL06 also computes the value of the infrared intensity for each normal mode, by computing the dipole moment variation along the normal mode adopting the Wannier set of localized functions[63−67]

The analysis of the computed frequencies for the 45S5 Bioglass structure has been carried out by means of three complementary methodologies: (i) the isotopic substitution of the atoms in the unit cell (^{48}Si for ^{28}Si, ^{36}O for ^{16}O, ^{51}P for ^{31}P, ^{53}Na for ^{23}Na, and ^{60}Ca for ^{40}Ca) to decouple frequencies; (ii) the potential energy distribution (PED), which is a vibrational analysis based on normal modes classification included in the CRYSTAL06 code; (iii) the graphical visualization of the displacements associated to the eingenvector of each mode using MOLDRAW code.[47] These techniques allowed us to distinguish different regions in the simulated IR spectrum.

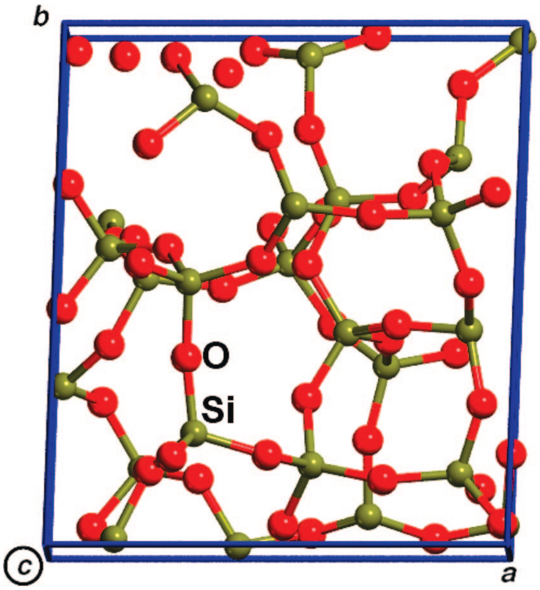

Figure 1. View along the c axis of the B3LYP v-SiO$_2$ optimized unit cell.

Results and Discussion

We present below our results for structure and dynamics of the glass systems studied. Our emphasis, however, is on the vibrational results; to this end, the structural data are presented in order to affirm the suitability of the model for the vibrational study. The results of structural and electronic studies of v-SiO$_2$ and 45S5 Bioglass have already been reported in previous papers[16,45,46] and will be briefly included here for the sake of completing the discussion of the vibrational features reported. We first discuss the structure, phonon, and IR spectra of v-SiO$_2$, which has been taken as a reference, and then turn our attention to the IR and phonon spectra of the 45S5 Bioglass.

Silica Glass. *Structure.* The structure of an amorphous all-silica model derived from the work of Bakos et al.[45,46] has been optimized at the B3LYP level with the same computational parameters adopted for the 45S5 Bioglass. The relaxed model, which has a unit cell of 72 atoms ($a = 9.75$ Å, $b = 11.00$ Å, $c = 10.43$ Å, $\alpha = 88.29°$, $\beta = 90.36°$, $\gamma = 87.92°$), is shown in Figure 1. The computed density of 2.139 g/cm^3 compares well with the experimental value of 2.2 g/cm^3.[68]

The average Si−O, O−O, and Si−Si distances of 1.636, 2.673, and 3.032 Å compare well with the experimental neutron diffraction data of 1.608, 2.626, and 3.077 Å[69] as well as the O−Si−O bond angle of 109.7° (109.5 ± 4° from

---

(54) Monkhorst, H. J.; Pack, J. D. *Phys. Rev. B.* **1976**, *8*, 5188.
(55) Hay, P. J.; Wadt, W. R. *J. Chem. Phys.* **1985**, *82*, 299.
(56) Hay, P. J.; Wadt, W. R. *J. Chem. Phys.* **1985**, *82*, 284.
(57) Habas, M. P.; Dovesi, R.; Lichanot, A. *J. Phys.: Condens. Matter* **1998**, *10*, 6897.
(58) Aprà, E.; Causà, M.; Prencipe, M.; Dovesi, R.; Saunders, V. R. *J. Phys.: Condens. Matter* **1993**, *5*, 2969.
(59) Dovesi, R.; FreyriaFava, C.; Aprà, E.; Saunders, V. R.; Harrison, N. M. *Philos. Trans. R. Soc. London, Ser. A* **1992**, *341*, 203.
(60) Dovesi, R.; Roetti, C.; Freyria Fava, C.; Prencipe, M.; Saunders, V. R. *Chem. Phys.* **1991**, *156*, 11.
(61) Lichanot, A.; Aprà, E.; Dovesi, R. *Phys. Status Solidi B* **1993**, *177*, 157.
(62) Prencipe, M.; Pascale, F.; Zicovich-Wilson, C. M.; Saunders, V. R.; Orlando, R.; Dovesi, R. *Phys. Chem. Miner.* **2004**, *31*, 1.
(63) Zicovich-Wilson, C. M.; San-Roman, M. L.; Camblor, M. A.; Pascale, F.; Durand-Niconoff, J. S. *J. Am. Chem. Soc.* **2007**, *129*, 11512.
(64) Baranek, P.; Zicovich-Wilson, C.; Roetti, C.; Orlando, R.; Dovesi, R. *Phys. Rev. B* **2001**, *64*, 125102.
(65) Noel, Y.; Zicovich-Wilson, C.; Civalleri, B.; D'Arco, P.; Dovesi, R. *Phys. Rev. B* **2002**, *65*, 014111.
(66) Zicovich-Wilson, C.; Bert, A.; Roetti, C.; Dovesi, R.; Saunders, V. R. *J. Chem. Phys.* **2002**, *116*, 1120.
(67) Zicovich-Wilson, C.; Dovesi, R.; Saunders, V. R. *J. Chem. Phys.* **2001**, *115*, 9708.
(68) Masatoshi, A.; Hannon, A. C.; Taylor, A. D.; Otomo, T.; Wright, A.; Sinclair, R. N.; Prrice, L. P. *Trans. Am. Crystallogr. Assoc.* **1991**, *27*, 113.
(69) Grimley, D. I.; Wright, A. C.; Sinclair, R. N. *J. Non-Cryst. Solids* **1990**, *119*, 49.

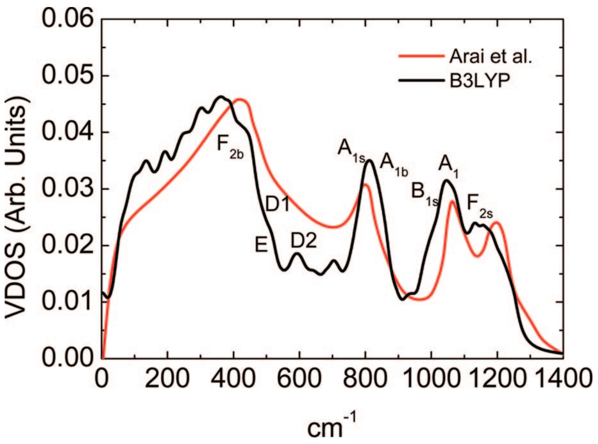

Figure 2. Experimental (red line) and B3LYP (black line) vibrational density of states of v-SiO$_2$.

neutron diffraction data) and the Si−O−Si bond angles of 141.9° compared to neutron diffraction data of 142.0° and NMR data of 146.7°.[70] The computed average Mulliken net charges are equal to 1.536e for Si and to −0.768e for oxygen resulting in a neutral SiO$_2$ unit.

Vibrational Density of States. The vibrational properties of v-SiO$_2$ have been extensively investigated by many experimental and some theoretical means.[71−88]

One of the most important quantities describing atomic dynamics, is the VDOS, defined as

$$g(\omega) = \frac{1}{3N}\sum_{j=1}^{3N} \delta(\omega - \omega_j) \tag{1}$$

where ω_j are the eigenvalues of the dynamical matrix.

To show the validity of the vibrational features of our model, in Figure 2 we report the calculated VDOS (broadened by Lorentzian functions with a typical width $\delta\nu = 40$ cm^{-1}) compared to the experimental one obtained by inelastic neutron scattering.[76]

A good agreement between the two is observed; shapes and positions of the principal peaks are well-reproduced. Two bands are clearly seen in the spectrum. The highest optical band has two pronounced peaks related to the stretching longitudinal and transverse vibrations of SiO$_4$ units. The structure of the lowest band is more complicated because of the overlap between acoustic and optical bands. In fact, structural disorder in glasses causes a broadening of the sharp band edges of crystals, transforming them in band tails. The main features of the VDOS shown in Figure 2 (a wide lower frequency band between 0−600 cm^{-1} and the narrow peaks at 800 cm^{-1} and 1100−1200 cm^{-1} separated by a gap of 200 cm^{-1}) are similar to those obtained for the different structural silica polymorphs[26,77,79,80] revealing that at least for ω > 200 cm^{-1}, g(ω) is dominated by the short-range aspect of the structure.

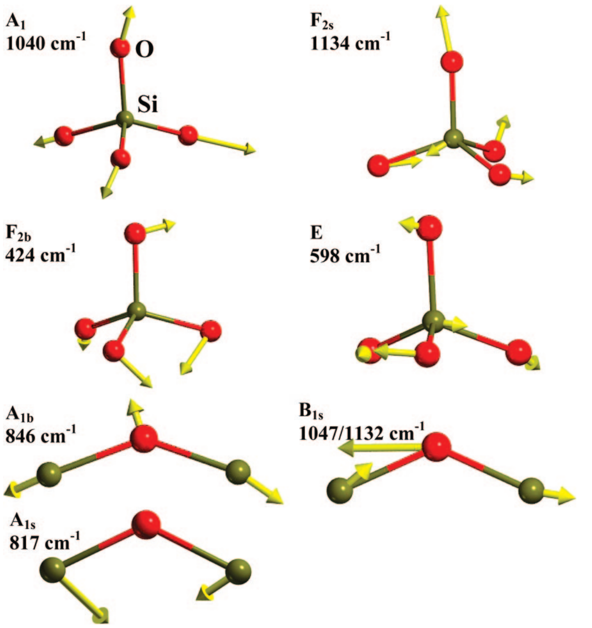

Figure 3. Schematic representation of the eigenmodes assigned to the SiO$_4$ and Si−O−Si structural units of v-SiO$_2$.

Vitreous silica can be imagined as being comprised of structural units of different types. The nonlinear three-atom Si−O−Si units and corner-shared tetrahedral SiO$_4$ units are usually considered to be the basic ones.[89] Therefore, the most convenient way to characterize the VDOS of the structure is to classify the vibrational modes in terms of internal vibrations of these structural units.[84] In the ideal case of isolated molecules, these structural units have the point-group symmetries C_{2v} and T_d, respectively. So, in Figure 3, we have labeled the vibrations of these units with different irreducible representations of the corresponding point group, following the classification reported by Taraskin et al.[84] However, it is worth noting that most of the vibrations cannot transform exactly like these irreducible species because of the complexity introduced by the network disorder.

The potential energy distribution analysis performed on the eigenvectors associated to each mode shows that the asymmetric stretching (B_{1s}) of Si−O−Si units gives dominant contributions to the eigenvectors characterized by frequencies in the region of the two high-frequency peaks in the VDOS at 1040 and 1140 cm^{-1}, whereas the Si−O−Si bending (A_{1b})

---

(70) Clark, T. M.; Grandinetti, P. J.; Florian, P.; Stebbins, J. F. *Phys. Rev. B* **2004**, *70*, 64202.
(71) Carpenter, J. M.; Price, D. L. *Phys. Rev. Lett.* **1985**, *54*, 441.
(72) Bell, R. J.; Dean, P. *Discuss. Faraday Soc.* **1970**, *50*, 55.
(73) Laughlin, R. B.; Joannopoulos, J. D. *Phys. Rev. B* **1977**, *16*, 2942.
(74) Sen, P. N.; Thorpe, M. F. *Phys. Rev. B* **1977**, *15*, 4030.
(75) Galeener, F. L.; Leadbetter, A. J.; Stringfellow, M. W. *Phys. Rev. B* **1983**, *27*, 1052.
(76) Arai, M.; Hannon, A. C.; Taylor, A. D.; Otomo, T.; Wright, A. C.; Sinclair, R. N.; Price, D. *Trans. Am. Crystallogr. Assoc.* **1993**, *27*, 113.
(77) Galeener, F. L.; Barrio, R. A.; Martinez, E.; Elliott, R. J. *Phys. Rev. Lett.* **1984**, *53*, 2429.
(78) Guttman, L.; Rahman, S. M. *Phys. Rev. B* **1986**, *33*, 1506.
(79) Ahmad, N.; Nex, C. M. M.; Phillips, W. A. *Philos. Mag. B* **1988**, *57*, 677.
(80) van Santen, R. A.; Vogel, R. A. *Adv. Solid State Chem.* **1989**, *1*, 151.
(81) Sanders, M. J.; Leslie, M.; Catlow, C. R. A. *J. Chem. Soc. Chem. Commun.* **1984**, *1271*, 1984.
(82) Feuston, B.; Garofalini, S. H. *J. Chem. Phys.* **1988**, *89*, 5818.
(83) Feuston, B.; Garofalini, S. H. *J. Phys. Chem.* **1989**, *91*, 564.
(84) Taraskin, S. N.; Elliott, R. J. *Phys. Rev. B* **1997**, *56*, 8605.
(85) Jin, W.; Vashishta, P.; Kalia, R. K.; Rino, J. P. *Phys. Rev. B* **1993**, *48*, 9359.
(86) Willson, M.; Madden, P. A.; Hemmati, M.; Angell, C. A. *Phys. Rev. Lett.* **1996**, *77*, 4023.
(87) Sarnthein, J.; Pasquarello, A.; Car, R. *Science* **1997**, *275*, 1925.
(88) Rahmani, A.; Benoit, M.; Benoit, C. *Phys. Rev. B* **2003**, *68*, 184202.
(89) Bell, R. J.; Dean, P. *Philos. Mag. B* **1972**, *25*, 1381.

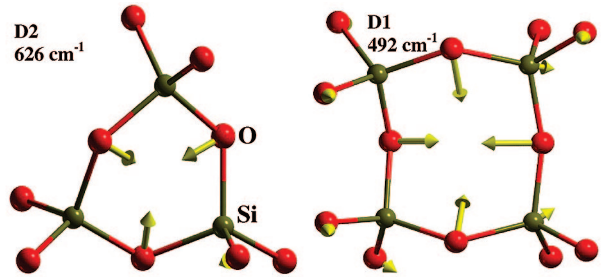

Figure 4. Breathing mode of the 3-ring (left) and 4-ring (right) assigned to the D2 and D1 peaks of the RAMAN spectrum.

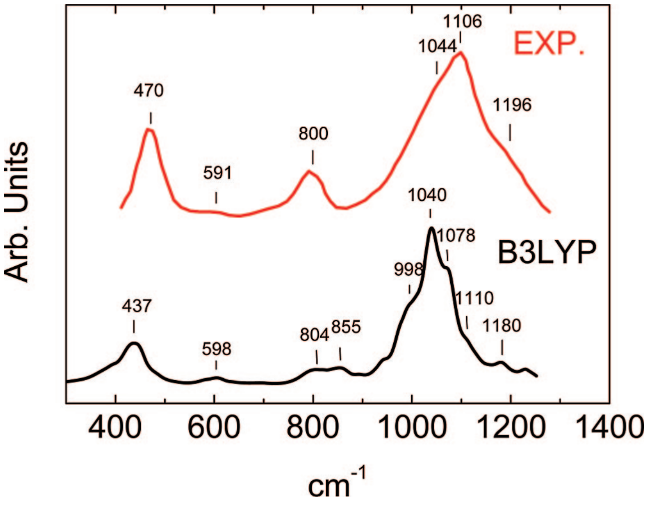

Figure 5. Experimental (red line) and B3LYP (black line) IR spectra of *v* SiO$_2$.

coupled with Si−O−Si symmetric stretching (A_{1s}) dominates in the range 600−850 cm^{-1}. On the other hand, for SiO$_4$ units, the symmetric stretching (A_1) contributes only to the eigenvectors characterized by the frequencies in the region of the lower peak at 1040 cm^{-1} in the high frequency band of the VDOS, the asymmetric stretching (F_{2s}) appreciably to the two high-frequency peaks in the VDOS at 1040 and 1140 cm^{-1} and slightly to the upper part of the lower band at 800 cm^{-1}, whereas the O−Si−O bending modes (F_{2b}, E) dominate in the middle of the lower band at around 400 cm^{-1} but still contribute up to 800 cm^{-1}.

The B3LYP VDOS also shows a shoulder at 492 and a peak at 626 cm^{-1} that are very close to the D1 (495 cm^{-1}) and the D2 (606 cm^{-1}) modes observed in RAMAN experiments which were ascribed to 3-fold and 4-fold rings.[77] The vibrational features of these rings inside the unit cell structure have been investigated by means of isotopic substitution procedure to decouple the eigenmodes associated to the rings from the surrounded network. Figure 4 shows the breathing modes of the 4-fold and 3-fold rings assigned to the D1 and D2 peaks. These breathing modes result from the bending modes of the Si−O−Si angles in 3-fold and 4-fold rings.

Infrared Spectrum. In Figure 5, the calculated IR spectrum of *v*-SiO$_2$ is compared to the experimental one[90] with good agreement. Three wide bands are clearly seen in the experimental spectrum at 470, 800, and 1106 cm^{-1}. However, in their work, Handke et al.[90] decomposed the original spectrum in 7 Gaussians centered at 470, 591, 733, 800, 1044, 1106, and 1196 cm^{-1}. The peak at 1044 cm^{-1} was ascribed to Si−O$^-$ defect vibrations while the peak at 1196 cm^{-1} was assigned to Si=O stretching vibrations. The computed spectrum shows peaks centered at 437 cm^{-1} assigned to O−Si−O bending, 598 cm^{-1} assigned to O−Si−O and Si−O−Si bendings, two peaks at 801 and 854 cm^{-1} assigned to O−Si−O and Si−O−Si bendings associated with Si−O symmetric stretching. The asymmetric Si−O−Si stretching vibrations are associated to the peaks at 998, 1040, 1078, 1110 and 1196 cm^{-1}. In contrast with experimental findings, the B3LYP spectrum reports the peak at 1040 cm^{-1} as the most intense rather than the one at 1106 cm^{-1} and no pronounced peaks are found at 733 cm^{-1}. Moreover, our calculations show that the band at 1044 and 1196 cm^{-1} cannot be considered as the evidence of Si−O$^-$ and Si=O defects because our free-defect model well-reproduces these bands.

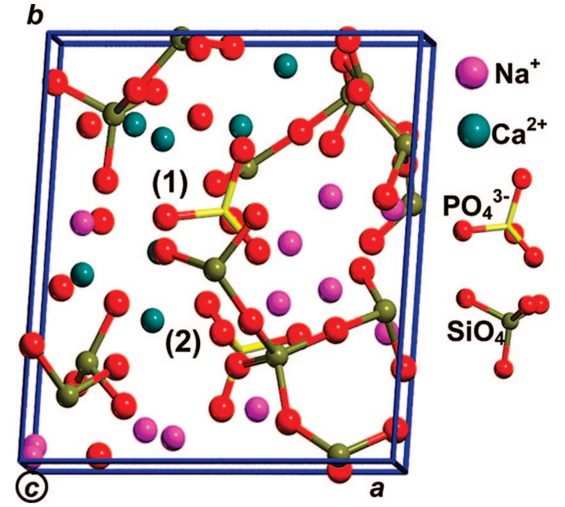

Figure 6. View along the *c* axis of the B3LYP Hench 45S5 Bioglass optimized unit cell. The unit cell contains 78 atoms with Na$_{12}$Ca$_7$P$_2$Si$_{13}$O$_{44}$ composition.

45S5 Bioglass. *Structure.* The 45S5 Bioglass model contains 78 atoms with composition Na$_{12}$Ca$_7$P$_2$Si$_{13}$O$_{44}$ (a = 9.42 Å, b = 10.24 Å, c = 10.34 Å, α = 88.7°, β = 91.7°, γ = 86.0°, density 2.82 g/cm^3) and it is shown in Figure 6. The fundamental structure of the Bioglass consists of a random network of distorted SiO$_4$ tetrahedra surrounded by sodium and calcium ions and of two phosphate groups, one isolated and the other linked to a SiO$_4$ group − in Figure 6 labeled (1) and (2), respectively. The intertetrahedral P−O distance of 1.55 Å is shorter than the Si−O distance which is 1.658 Å. Moreover, P−NBO bonds (1.54 Å) are significantly shorter than Si−NBO bonds (1.60 Å), and P−BO bonds (1.65 Å) are also shorter than Si−BO bond (1.67 Å). These results show that the different strength of T−BO and T−-NBO bond (T = Si/P) is well-reproduced in our simulations.

The average O−Si−O and O−P−O bond angles are centered at the tetrahedral angle of 109.4 and 109.5°, respectively. Calcium is 6-fold coordinated with average

---

(90) Handke, M.; Mozgawa, W.; Nocun, M. *J. Mol. Struct.* **1994**, *325*, 129.

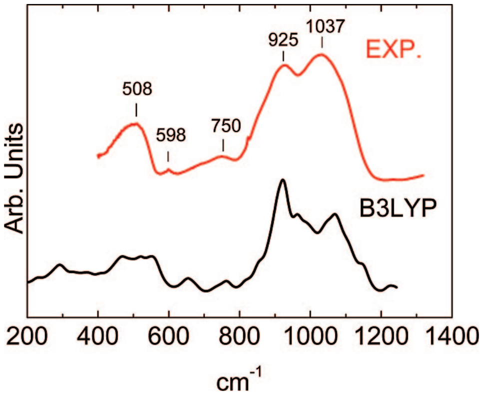

Figure 7. Experimental (red line) and B3LYP (black line) IR spectra of 45S5 Bioglass.

distances of 2.44 Å, whereas sodium is surrounded by 5.3 oxygens with average distances of 2.36 Å.

Finally, the average Si−O−Si and Si−O−P angles are 135.6 and 138.0°, respectively. The local structure of the Bioglass is similar to that of the crystal phases obtained after thermal treatment, namely, $Na_2CaSi_2O_6$ and β-$NaCaPO_4$.[15] It is worth mentioning that the average distances reported above are not directly comparable to those extrapolated from the radial distribution functions coming from Carr−Parrinello molecular dynamics simulations in which thermal motion is considered. Mulliken net charges are close to the formal ionic charges (average values are 0.872, 2.054, −2.887, and −2.333 electrons for Na, Ca, PO_4(1), and PO_4(2), respectively) showing the ionic nature of the Bioglass, whereas the large band gap of 6.5 eV shows, as expected, its strong insulating character. A detailed discussion of structural and electronic features of the 45S5 Bioglass was reported in a recent paper.[16]

Infrared Spectrum: Experiment vs B3LYP. In Figure 7, the calculated IR spectrum (broadened by Lorentzian functions with a typical width $\delta\nu = 40$ cm^{-1}) is compared to the experimental one.[91] Both the adsorption spectra show the same bands at 1037, 925, 753, 600, and 500 cm^{-1}, with the experimental spectrum being more broadened. From an experimentalist point of view, these wide bands are assigned as follows: the band at 1037 cm^{-1} is associated with the asymmetric stretching of bridging oxygens (Si−BO−Si) in all Q species, the band at 925 cm^{-1} is assigned to the Si−NBO stretching vibrations in SiO_4 and it covers P−NBO stretching vibrations in PO_4 tetrahedra. The band around 600 cm^{-1} is assigned to the symmetric stretching vibrations of three membered siloxane rings of SiO_4 and to the O−P−O bending vibration in a PO_4 tetrahedra, whereas the wide peak at 500 cm^{-1} is associated to O−Si−O bending vibrations in SiO_4 and symmetric oxygen stretching of Si−O−Si.

Isotopic Substitutions. From this preliminary discussion, the complexity of the infrared spectrum of 45S5 Bioglass is evident. Important information on which ions are involved in the vibrational modes of different regions of the spectrum, which is entirely lacking from the sole experimental evidence, can be inferred theoretically by proper isotopic substitutions. By changing the reduced mass of an element, its motion is decoupled from the other atoms with a shift in frequencies ($\Delta\nu$) proportional to the change in mass and to its involvement in the normal mode. In this work, different isotopic masses have been tried and the best substitutions resulted ^{53}Na for ^{23}Na, ^{60}Ca for ^{40}Ca, ^{51}P for ^{31}P, and ^{48}Si for ^{28}Si. It should be clear that these choices were guided by the convenience in the resulting shifts, not referring to any experimental comparison.

Figure 8 shows the resulting frequency shift ($\Delta\nu$) with respect to the pristine frequency (ν), expressed in cm^{-1}, for the considered elements. The modes involving sodium atoms lie in the range 40−400 cm^{-1} with maximum shifts of 30 and 27 cm^{-1} associated with the frequency at 167 and 227 cm^{-1}, respectively.

Modes involving calcium atoms lie in the range 47−570 cm^{-1} with maximum ($\Delta\nu = 13$ cm^{-1}) at 273 cm^{-1}. These findings are in nice agreement with far-infrared spectra of soda-silicate and soda-lime glasses which exhibit a band, called cation mode, characteristic of the interaction between alkali atoms, and the NBO atoms in the glass network. The frequency of this band is weakly dependent on the nature of the network forming ion (Si, V, B, P, and Ge) but it is strongly dependent on the nature of the modifier cations.[92] The peak of calcium is found[93] around 250 cm^{-1}, whereas sodium shows[94] a maximum at 180 cm^{-1}.

In Figure 8, the isotopic substitution has been used to differentiate the two phosphate groups inside the Bioglass unit cell. Values of nonsubstituted frequencies are indicated in correspondence with the maximum shift computed after substitution. In the case of isolated phosphorus P(1), the maximum shift is 70 cm^{-1} and affects the P(1)═O stretching (1222 cm^{-1}). Another largely shifted frequency is at 1147 cm^{-1} ($\Delta\nu = 23$ cm^{-1}), which corresponds to a combined P−O and Si−O stretching mode and the frequency at 648 cm^{-1} which undergoes a shift of 22 cm^{-1} can be assigned to the O−P(1)−O bending mode. Finally, in the region around 900 cm^{-1}, many frequencies are altered because of the presence of P(1) stretching modes combined with other modes.

The same analysis carried out on the phosphate linked to the silica network, P(2), shows that the maximum shift ($\Delta\nu = 68$ cm^{-1}) affects the P(2)═O stretching mode at 1242 cm^{-1}. The P(2)−BO−Si stretching mode, located at 885 cm^{-1} in the spectrum of the nonsubstituted structure, shifts 18 cm^{-1}, whereas the frequency at 624 cm^{-1} assigned to the O−P(2)−O bending mode is shifted 13 cm^{-1}. Moreover, a region with small shifts is present in the range 500−700 cm^{-1} in which the Si−O−P(2) bending modes are involved.

The isotopic substitution of ^{48}Si/^{28}Si offers a very complex situation. In fact, as it is clear from the graph of Figure 8, silicon is involved in the great majority of vibrational modes. It is worth noting that the only region free from silicon shifts is at frequency values higher than 1150 cm^{-1}. In that region,

---

(91) Lusvardi, G.; Malavasi, G.; Menabue, L.; Menziani, M. C.; Pedone, A.; Segre, U.; Aina, V.; Perardi, A.; Morterra, C.; Boccafoschi, F.; Gatti, S.; Borsetti, M.; Cannas, M. *J. Biomater. Appl.* **2008**, . in press.

(92) Exarhos, G., Jr *Solid State Commun.* **1972**, *11*, 755.

(93) Gervais, F.; Lagrange, C.; Blin, A.; Aliari, M.; Hauret, G.; Coutures, J. P.; Leroux, M. *J. Non-Cryst. Solids* **1990**, *119*, 79.

(94) Hauret, G.; Vaills, Y.; Parot-Rajaona, T.; Gervais, F.; Mas, D.; Luspin, Y. *J. Non-Cryst. Solids* **1995**, *191*, 85.

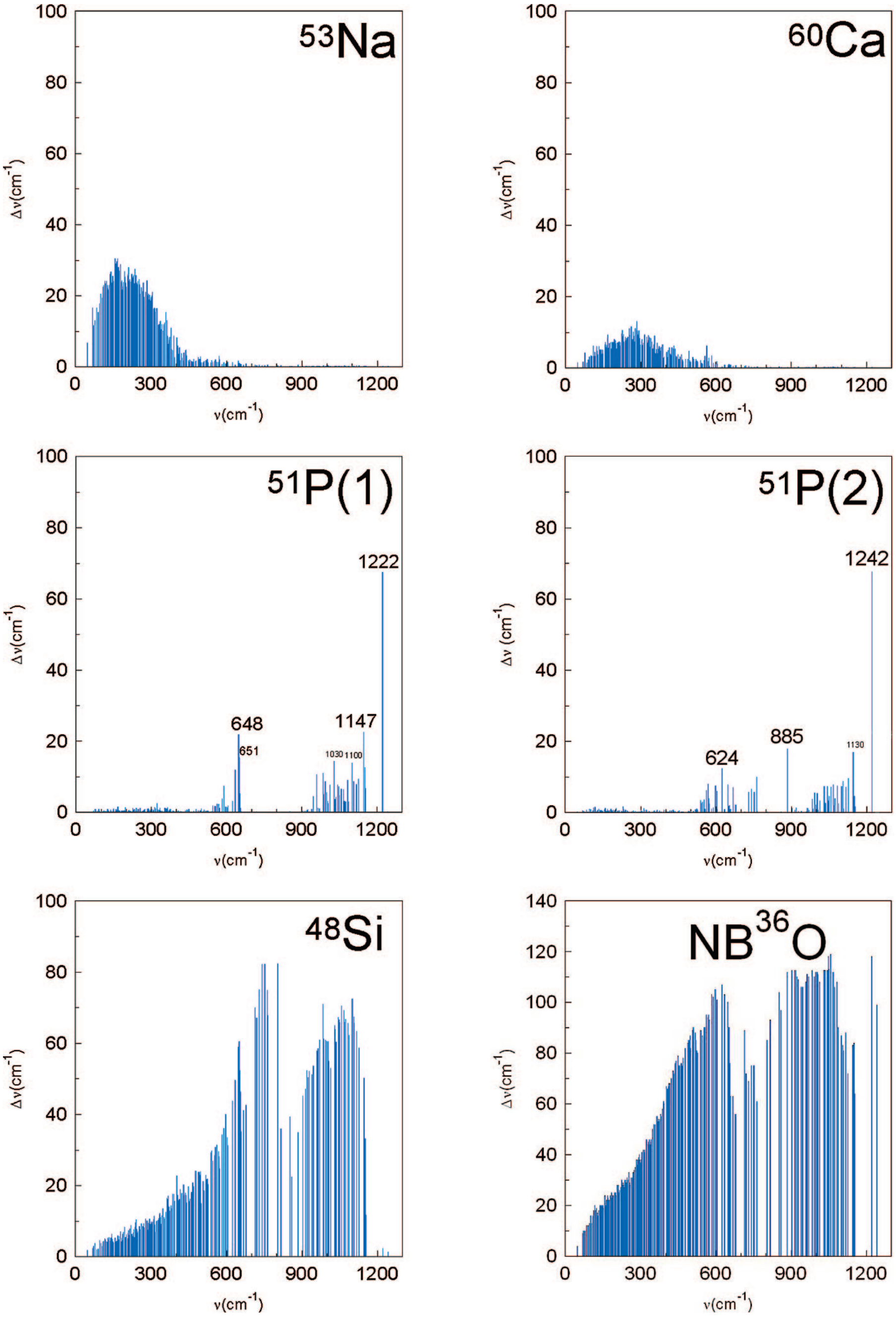

Figure 8. Bioglass isotopic shift (Δν, cm^{-1}) suffered by the vibrational frequency ν upon ^{53}Na/^{23}Na, and ^{60}Ca/^{40}Ca (first two graphs), ^{51}P/^{31}P for both isolated P1 and linked to the framework P2 (second row), ^{48}Si/^{28}Si and NB^{36}O/NB^{16}O (last two graphs).

only P−O stretching modes are involved. Moreover, in the region between 10 and 100 cm^{-1}, in which modifier cations are vibrating, the shifts are very small, indicating that the vibrational modes of the silica network are influenced by sodium and calcium dynamics.

Finally, it has been useful to substitute oxygen atoms of the NBO type, according to ^{36}O/^{16}O as in Figure 8. It resulted that NBO is involved in the whole spectral region, a part from the very high frequencies, where P(2)−O stretching modes are present. In that region, above 1200 cm^{-1}, only stretching modes of the isolated P−O are affected by the isotopic substitution. The maximum isotopic shift ($\Delta\nu = 123$ cm^{-1}) is associated to the original frequency of 914 cm^{-1}, which in the IR spectrum is covered by the more intense peak at 924 cm^{-1}, related to NBO−Si−NBO stretching vibrations, as is discussed in the following section.

Band Assignment of the IR Spectrum. A more detailed comprehension of the vibrational modes associated to the IR spectrum can be performed by the potential energy distribution analysis and graphical visualization of the eigenvectors associated to the different modes.

Because our structural model has 78 atoms in the unit cell with P1 symmetry, it shows 78 × 3 = 234 degrees of freedom, 231 of which have vibrational character. Among all these modes, only a small amount of peaks are clearly distinguishable in the computed IR spectrum broadened by Lorentzian functions with a typical width $\delta\nu = 20$ cm^{-1}, reported in Figure 9. Therefore, only these vibrational modes will be discussed in the following.

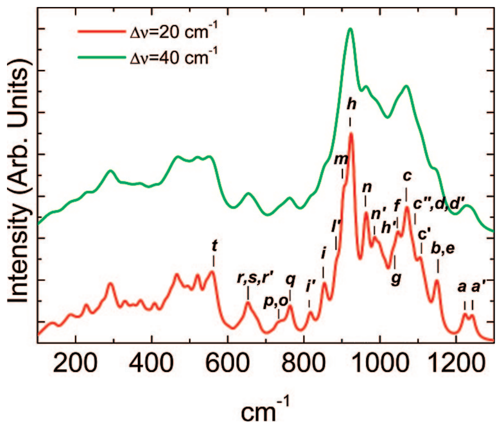

Figure 9. Computed IR spectra broadened by Lorentzian functions with a typical width $\delta\nu = 20$ and 40 cm^{-1}. Letters refer to text and Figure 10.

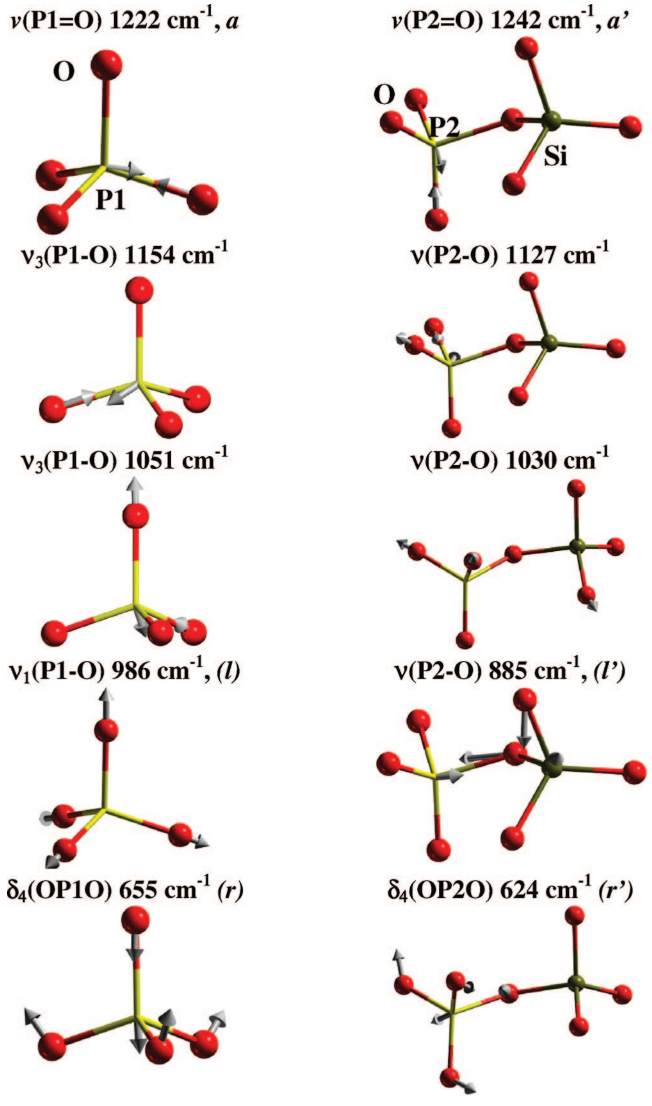

Figure 10. Schematic representation of the eigenmodes assigned to the different PO_4 structural units of 45S5 Bioglass. P1 indicates the isolated phosphate (left), whereas P2 indicates that linked to the framework (right). Letters refer to text and Figure 9.

Figure 9 shows that the band at 1075 cm^{-1} in the $\Delta\nu =$ 40 cm^{-1} broadened spectrum covers at least 6 peaks. This also holds for the experimental spectrum. In fact, the tail of the experimental spectrum can hide the small doublet peak beyond 1200 cm^{-1} which is assigned to the stretching of the P(1)=O (1222 cm^{-1}) (*a*, Figures 9 and 10) and P(2)=O (1242 cm^{-1}) (*a′*, Figures 9 and 10) double bonds. The peak at 1147 cm^{-1} is assigned to the asymmetric Si−BO stretching of a Q^4 species linked to a Q^2 species sporting a Si−BO−Si angle close to 180°(*b*, Figure 9). The major peak at 1075 cm^{-1} (*c*, Figure 9) and the two peaks at 1107 (*c′*) and 1088 cm^{-1} (*c″*) are assigned to an asymmetric Si−$(NBO)_2$ stretching vibration of a Q^2 species. These peaks cover two other intense peaks at 1070 *(d)* and 1067 *(d′)* cm^{-1} assigned to the asymmetric Si−BO−Si stretching vibrations of a Q^2 species linked to a Q^2 and a Q^3 species, respectively. The Si−NBO stretching mode at 1108 cm^{-1} associated to a Q^3 species is also covered by this band (*e*, Figure 9).

The peak at 1047 cm^{-1} is associated with an asymmetric Si−BO−Si stretching vibration of a Q^4 species connected to a Q^1 species (*f*, Figure 9) and covers the Si−NBO stretching vibration of a Q^1 species at 1014 cm^{-1} (*g*).

The band centered at 924 cm^{-1}, which is assigned to a symmetric NBO−Si−NBO stretching vibration of a Q^2 species (*h*, Figure 9), covers several peaks in the IR spectrum of Figures 7 and 9. In particular, the peaks at 853, 885, 904, 964, and 985 cm^{-1} are hidden. The peaks at 853 (*i*) and 817 (*i′*) cm^{-1} are assigned to an asymmetric Si-BO-Si asymmetric stretching of a Q^2 species connected to another Q^2 species. The peak at 885 cm^{-1} is assigned to the asymmetric P−BO−Si stretching of the PO_4 unit connected to the network (*l′*, Figure 9 and 10), whereas the peak a 904 cm^{-1} is assigned to an symmetric Si−BO−Si stretching of a Q^3 species connected to a Q^2 species (*m*, Figure 9). The peaks at 964 and 985 cm^{-1} are assigned to the asymmetric Si−$(NBO)_3$ stretching of a Q^1 species (*n* and *n′*, Figure 9). The latter covers a symmetric Si−$(NBO)_2$ stretching of a Q^2 species at 998 cm^{-1}(*h′*, Figure 9).

Figure 10 reports the schematic representation of the eigenmodes assigned to the different PO_4 structural units of 45S5 Bioglass. The isolated PO_4 unit sports stretching vibrations at 1222, 1154, 1051, and 986 cm^{-1}, whereas the PO_4 unit linked to the network sports stretching vibrations at 1242, 1127, 1030, and 885 cm^{-1}.

The weak P−O stretching vibrational mode (υ_3, Figure 10) of the PO_4 unit occurs in the range 1029−1151 cm^{-1} and, because this model is superimposed with the strong vibrational mode of the Si−O bonds discussed above, it is hard to distinguish the P−O vibration from the Si−O one at low content of phosphorus. The symmetric (υ_1) stretching mode is found at 986 cm^{-1} (*l*, Figure 10) in the isolated PO_4 unit but with a very weak intensity as expected since it is only Raman active when PO_4 is in the free ion state. Among these stretching vibrations, only the peak at 885 cm^{-1} associated to the P−O−Si stretching mode shows a medium intensity and it could be considered a typical marker for Si−O−P bonds in the structure (*l′*, Figures 9 and 10).

In the range 600−800 cm^{-1}, two main peaks are present, at 750 and 655 cm^{-1}. The peak at 750 cm^{-1} is assigned to a BO−Si−BO bending vibration (*o*, Figure 9) while the bump at 730 cm^{-1} is assigned to the symmetric Si-BO-Si stretching vibration (*p*, Figure 9). The peak at 655 cm^{-1} is associated to the O−P(1)−O bending vibration (δ_4) (*r*,

Table 1

mode	B3LYP	IR intensity
ν'(P2=O)	1242 (*a′*)	vw
ν (P1=O)	1222 (*a*)	vw
ν (Si−BO) $Q^4 - Q^2$	1147 (*b*)	w
ν (Si−NBO) Q^3	1108 (*e*)	w
ν (Si−NBO) Q^2	1107 (*c′*)	w
ν_a (Si−$(NBO)_2$) Q^2	1088 (*c″*)	m
ν_a (Si−$(NBO)_2$) Q^2	1075 (*c*)	m
ν_a (Si−BO−Si) $Q^2 - Q^2$	1070 (*d*)	m
ν_a (Si−BO−Si) $Q^2 - Q^3$	1067 (*d′*)	m
ν_a (Si−BO−Si) $Q^4 - Q^1$	1047 (*f*)	m
ν (Si−NBO) Q^1	1014 (*g*)	w
ν_s (Si−NBO) Q^2	998 (*h′*)	m
ν_s (P1−NBO)	986 (*l*)	vw
ν_a (Si−$(NBO)_3$) Q^1	985 (*n′*)	m
ν_a (Si−$(NBO)_3$) Q^1	964 (*n*)	m
ν_s (NBO−Si−NBO) Q^2	924 (*h*)	vs
ν_a (Si−BO−Si) $Q^3 - Q^2$	904 (*m*)	s
ν_a (P2−BO−Si)	885 (*l′*)	m
ν_a (Si-BO-Si) $Q^2 - Q^2$	853 (*i*)	w
ν_a (Si−BO−Si) $Q^2 - Q^2$	817 (*i′*)	w
δ (BO−Si−BO) Q^4 + ν_a (Si−BO−Si)	763 (*q*)	vw
δ (BO−Si−BO)	750 (*o*)	vw
ν_s (Si−BO−Si)	730 (*p*)	vw
δ (OP1O)	655 (*r*)	w
δ (OSiO)	648 (*s*)	w
δ (OP2O)	624 (*r′*)	vw
δ (OSiO) Q^2 + ν (Ca−NBO)	562 (*t*)	w
δ (O−Si−O) Q^2	521	w
δ (OCaO) + δ (ONaO) + δ (OSiO) Q^1	494	w
δ (O−Si−O) Q^3	466	w
ν (Ca−NBO)	556, 507, 499, 461, 453, 409	w
ν (Na−NBO)	371, 297, 246, 241, 197, 158	w
ν (Na−NBO−-Si) Q^3	287	vw

Figures 9 and 10) and it covers the O−Si−O bending mode at 648 cm^{-1} *(s)* and the O−P(2)−O bending vibration at 624 cm^{-1} (*r′*, Figures 9 and 10). The peak at 562 cm^{-1} is assigned to the O−Si−O bending mode and the Ca−NBO stretching vibrations (*t*, Figure 9). Pure Ca−O stretching vibrations contribute to the peaks at 556, 507, 499, 461, 453, and 409 cm^{-1}. The Na−O stretching modes are involved in a lower region, i.e. between 100 and 300, prevalently at 158, 197, 241, 246, 297, 371 cm^{-1}. O−Ca−O bending modes (290 cm^{-1}) are strongly coupled with O−Na−O bending modes (224, 307, and 315 cm^{-1}) in the region between 100 and 400 cm^{-1}. A peak at 498 cm^{-1} is the result of these two bending motions, together with the O−Si−O bending of a Q^2 species. Table 1 summarizes the vibrational modes of the B3LYP 45S5 IR spectrum reported in Figures 7, 9, and 13.

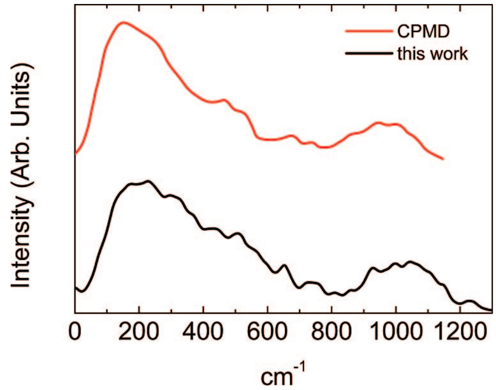

Figure 11. 45S5 Bioglass B3LYP vibrational density of states (black line) compared to the one obtained by Carr−Parrinello Molecular Dynamics (CPMD) simulations[22] (red line).

Vibrational Density of States: B3LYP vs CPMD. In Figure 11 the VDOS computed at B3LYP level is compared to the one calculated as Fourier transform of the velocity autocorrelation function (VACF) obtained by Carr−Parrinello Molecular Dynamics by using the generalized gradient approximation (GGA) and the PBE exchange-correlation functional.[95] As discussed by Tilocca et al. and reported in Table 1, the bottom part of the spectrum is dominated by the low frequency oscillations (100−400 cm^{-1}) of Na and Ca ions around their NBO sites, with calcium vibrating at a slightly higher frequency. The region between 400 and 800 cm^{-1} is associated with O−Si−O, O−P−O, and Si−O−Si bending vibrations in silicate glasses. The two approaches are in nice agreement, with the latter showing a red shift of the high-frequency band that ranges between 800 −1100 cm^{-1}. Finally, Tilocca has reported a possible marker of Si−O−P linkage at 670 cm^{-1}, though it is visible in the form of a high-frequency shoulder in the Si−O stretching band. Among our computed frequencies, at 668 cm^{-1} there is the Si−O−Si bending of the Si linked to P, which is a bump in the peak at 651 cm^{-1}.

However, in the case of IR spectrum, another possible and more direct marker of P−O−Si bonds can be the peak at 885 cm^{-1} (medium intensity) which is shifted of about 100 cm^{-1} with respect to the mode of the isolated PO_4 (986 cm^{-1}).

In their work Tilocca et al.[24] also projected the VDOS onto different Q^n(Si) sites showing that the two high-frequency peaks correspond to the dominant Q^2 species. Q^4 species showed a single peak at 1010 cm^{-1}, whereas orthosilicate Q^0 showed a single peak at 890 cm^{-1}.

To study the contribution of different Q^n(Si) sites in our spectrum we employed the isotopic substitution techniques. In our approach, the different Q^n species and their oxygens of the SiO_4 tetrahedron have been isolated by changing silicon and oxygen masses according to the formula $^{48}Si\,^{36}O_4$. The full IR spectrum has then been computed for each case. The corresponding frequency shifts of the obtained values after isotopic substitutions with respect to the original values give an estimate of the relative contributions of the various Q^n species to the spectrum. Figure 12 shows four graphs, one for each Q^n type present in the structure, where isotopic shifts ($\Delta\nu$) are plotted in function of the original frequencies ν. It is clear that Q^2 species are dominant in the spectrum, both for number and intensity of the frequencies shifted (in Figure 12 first row, rightmost), because the maximum shift $\Delta\nu$ is 240 cm^{-1} associated to the frequency at 985 cm^{-1}. Also much shifted are normal modes in the region between 860 and 1100 cm^{-1} with $\Delta\nu$ larger than 70 cm^{-1} in agreement with Tilocca's findings. Moreover, the Q^2 species show discrete shifts also in the low frequency region, that is between 300 and 500 cm^{-1}. The Q^4 species have a less intense maximum shift ($\Delta\nu$ = 148 cm^{-1}) in correspondence to the frequency of 914 cm^{-1} and generally the largest shifts are in the region between 750 and 1000

---

(95) Perdew, J. P.; Burke, K.; Ernzerhof, M. *Phys. Rev. Lett.* **1996**, *77*, 3865.

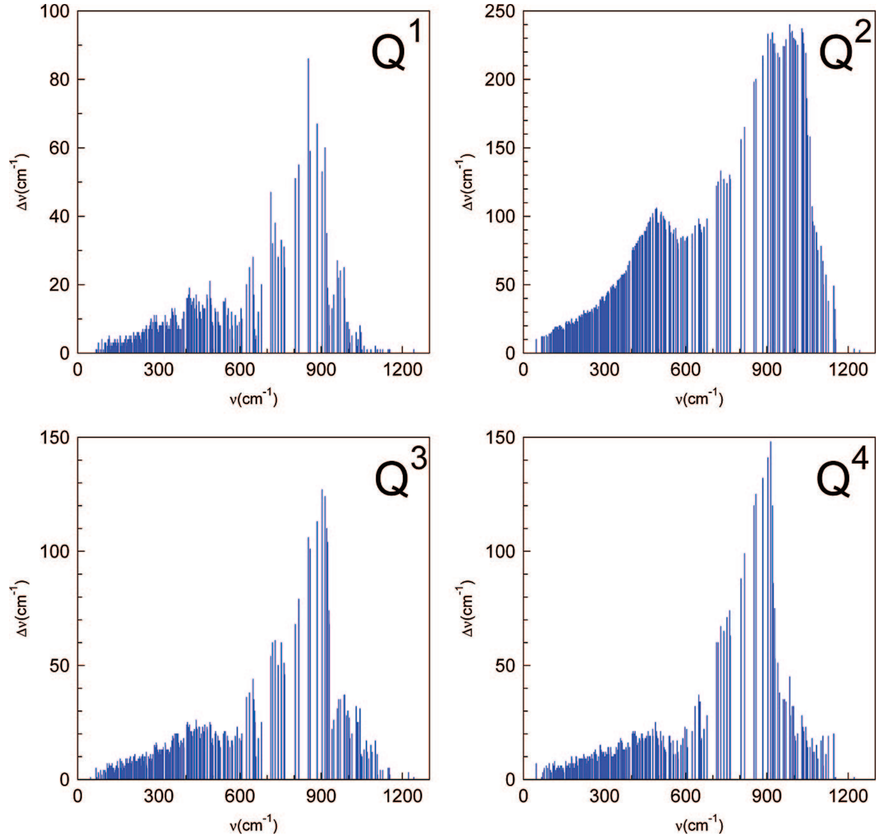

Figure 12. Bioglass isotopic shift (Δν, cm^{-1}) suffered by the vibrational frequency ν upon ^{48}Si^{36}O$_4$/^{28}Si^{16}O$_4$ substitution for Q^1, Q^2 (first row) and Q^3, Q^4 species (last row).

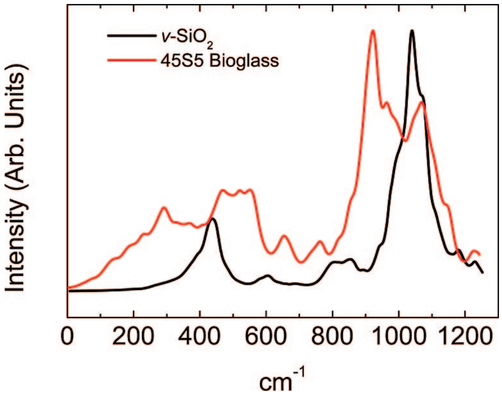

Figure 13. Comparison between IR spectra of 45S5 Bioglass (red line) and υ-SiO$_2$ (black line).

cm^{-1} (Figure 12, second row, rightmost). The Q^3 species show a maximum shift of 127 cm^{-1} corresponding to the original frequency of 904 cm^{-1} and the most shifted modes are those in the region between 700 and 930 cm^{-1} (Figure 12, second row, leftmost). Finally, the Q^1 species is present in a very low amount inside the structure and its maximum shift ($\Delta\nu = 87$ cm^{-1}) affected the frequency at 853 cm^{-1}, the other significant shifts being in the region between 650 and 900 cm^{-1} (Figure 12, first row, leftmost).

Comparison between 45S5 and υ-SiO$_2$ IR Spectra. Finally, Figure 13 shows the direct comparison of the IR spectra of υ-SiO$_2$ and 45S5 Bioglass, both computed at the B3LYP level. Most intense peaks are shifted by the effect of the presence in the silica network of Ca^{2+} and Na$^+$ modifiers. Particularly, in the 45S5 case, in the region between 850 and 1200 cm^{-1}, a double peak and a shoulder are found, whereas in the silica spectrum there is the Si−O stretching peak. Bands characteristic for [SiO$_4$]$^{4-}$ and [PO$_4$]$^{3-}$ tetrahedra occur in similar spectral range, except for the *P*=O stretching modes, present in the Bioglass spectrum at high frequency (1200−1250 cm^{-1}) and absent in the silica case. In the region around 900 cm^{-1}, the presence of modifiers is revealed by the vibrations of broken silicon oxygen bridges with the formation of Si-NBO bonds. In the low frequency region of the spectrum (100−600 cm^{-1}), the single peak present in case of υ-SiO$_2$ is replaced by broad bands due to stretching vibrations of Ca−O and Na−O stretching modes. O−Si−O bending modes in the Bioglass are shifted at higher frequencies than in silica.

Conclusions

In this work, the structure and vibrational features of a model of an amorphous υ-SiO$_2$ glass have been compared with that of a corresponding model for the Hench's 45S5 Bioglass (of composition 46.1 SiO$_2$, 24.4 Na$_2$O, 26.9 CaO and 2.6 P$_2$O$_5$ mol %). Ab initio periodic calculations based on the rather accurate B3LYP hybrid functional have been performed using a Gaussian basis set of double-ζ plus polarization quality in a periodic fashion as coded in the CRYSTAL06 program. A unit cell envisaging 78 atoms (P1 space group) derived by a structure properly quenched via a classical molecular dynamics protocol has been adopted as the initial geometrical guess for a full B3LYP periodic structural optimization. On the optimum structure, the harmonic vibrational spectrum has been computed by diagonalizing the weighted Hessian matrix associated with the central zone. Both the resulting structures and vibrational features have been shown to be in excellent agreement with the experimental data and with literature vibrational spectrum computed by plane wave calculations and Fourier transform of the velocity autocorrelation function. This clearly proves that the harmonic approximation is an excellent approximation for systems containing only relatively heavy atoms (O, P, Si, Na, and Ca in the Hench's glass) and no hydrogen atoms (for which anharmonicity is relevant), as it is the case here. The proposed approach is shown to be very powerful, because by a combination of tools (potential energy distribution and isotopic substitution, both automatically provided by the CRYSTAL06 code and graphical analysis of the normal eigenvectors) each vibrational band has been characterized in terms of meaningful internal geometrical deformations associated to the normal mode, allowing a full assignment and interpretation of the experimental bands. This fact is extremely important, particularly for system like those considered here, in which the amorphous nature of the material and the lack of symmetry hamper the detailed understanding of the experimental features. For the first time, the direct comparison of the computed infrared spectrum of a pure v-SiO_2 glass have been carried out with that of a corresponding model for the Hench's 45S5 Bioglass, allowing a microscopic understanding of the role of Na^+ and Ca^{2+} modifiers on the vibrational features of a bioglass.

An important issue in bioglass science involves the partial incorporation of phosphate units into the silicate network, which may affect the phosphate release rate. Our approach supports this incorporation. The low percentage of phosphate in these glasses might hinder the detection of P−O−Si features in IR and RAMAN spectra. However, the detailed assignment of vibrational features in the IR spectrum allows us to identify a possible marker of P−O−Si bonds: for instance, the peak at 885 cm^{-1} (medium intensity) which is shifted of about 100 cm^{-1} with respect to the mode of the isolated PO_4 (986 cm^{-1}). Because its intensity overlaps with the silicate intensity in this region, this peak is still hard to detect in the spectrum at least for low P-content.

These excellent results also show that the simulation of the static (structures) and dynamic (infrared and Raman spectra) features of a truly amorphous material can be successfully simulated ab initio without resorting to extremely large unit cells, as in this study only about 80 atoms defined the unit cell contents for v-SiO_2 glass and Hench's 45S5 Bioglass. Because all the CRYSTAL06 calculations reported in this work were run on commodity clusters envisaging 16 CPUs as a maximum (2 Gbyte RAM per node), this opens up the possibility to predict complex phenomena occurring in these materials (cation substitution, defect formation, surface modeling, etc.) at a modest cost compared to the corresponding experimental approach. At the moment, thanks to both the updating process in the CRYSTAL06 code and improved hardware facilities, unit cells including twice as many atoms than the present ones have already started to be studied to understand the role of higher phosphorus content on the physico chemical features of these important biomaterials.

Acknowledgment. Financial support from the Italian Ministry MIUR (Project COFIN2006, Prot. 2006032335_005 led by Prof. C. Morterra) and from the Regione Piemonte (Bando ricerca scientifica Piemonte 2004, Settore: Nanotecnologie e nanoscienze, “Materiali nanostrutturati biocompatibili per applicazioni biomediche”, led by Prof. C. Morterra) is gratefully acknowledged. We thank Prof. S. Pantelides for kindly providing the coordinates of the starting structure of the v-SiO_2 glass.

CM801164U